Deformation of Carbon Nanotubes by Exposure to Water Vapor

Maria Pia Rossi,[†,§] Yury Gogotsi,[†] and Konstantin G. Kornev*[,‡]

Department of Materials Science and Engineering and A. J. Drexel Nanotechnology Institute, Drexel University, 3141 Chestnut Street, Philadelphia, Pennsylvania 19104, and School of Materials Science and Engineering, Clemson University, 161 Sirrine Hall, Clemson, South Carolina 29634-0971

Received August 17, 2008. Revised Manuscript Received December 16, 2008

The condensation of water inside multiwalled carbon nanotubes has been monitored and controlled using environmental scanning electron microscopy. Undersaturated vapor condenses inside nanotubes and forms nanometer-thick water films. Simultaneously, nanotubes deform and decrease their apparent diameter. When the vapor pressure in the chamber approaches the saturation pressure, we observe the formation of menisci and spontaneous buckling of the nanotubes. We derive a criterion of the buckling instability caused by capillary condensation. Remarkably, the buckling criterion appears to be independent of the meniscus shape. Using our experiments and models, we estimated the circumferential Young's modulus of large-diameter carbon nanotubes with disordered wall structure produced by the chemical vapor deposition method (CVD) to be $E_{\theta\theta} \approx 13-18$ MPa. It appears to be at least 2 orders of magnitude lower than the longitudinal modulus of nanotubes produced by arc discharge or catalytic CVD methods. The reported experiments and proposed theory suggest possible applications of "soft" nanotubes as sensors to probe minute concentrations of absorbable gases and vapors.

Introduction

Interest in the behavior of fluids inside nanochannels has greatly increased within the scientific community over the past decade.[1] The field of nanofluidics promises to produce tools that would enable applications ranging from single-molecule transport[2] to delivering therapeutic solutions to individual cells.[3,4] Much effort has been dedicated, in particular, to the study of the fluid behavior inside carbon nanotubes (CNTs).[5] Because of their reported superior mechanical, electrical, and physical properties,[6,7] CNTs could be ideal as tools for controlled fluid delivery on the nanoscale. However, because devices using CNTs as nanopipettes are being developed,[8,9] their interaction with fluids and their capacity for liquid delivery must be well characterized and understood.

Although much work has centered around predicting the behavior of fluids on the nanoscale through computational simulations and theoretical analysis,[1,10−14] limited experimental data has been shown. Many of the experimental observations of liquids inside CNTs such as neutron scattering,[15] X-ray diffraction,[16] or vibrational spectroscopy[17] did not allow for visualization. Nonetheless, the visualization of fluids inside CNTs has been reported using transmission electron microscopy (TEM) of capped CNTs,[18,19] optical microscopy,[20] or environmental scanning electron microscopy (ESEM) of open-ended CNTs.[21] Although TEM enables the study of fluids inside CNTs with very small internal diameters (∼2−4 nm), the fact that these have to be capped to withstand the high vacuum of the instrument limits observations to phase changes of organic and aqueous fluids trapped inside closed CNTs. Optical microscopy enables observations at room temperature and ambient pressure but does not provide high-magnification images of menisci inside CNTs. ESEM, however, enables the observation of fluids inside CNTs at high magnification inside its low-vacuum environmental chamber, which affords pressures of up to 20 Torr and temperature control using a Peltier cooling stage.[22,23]

Water condensation and evaporation have been induced within the hollow cavities of open CNTs by controlling the pressure and temperature inside the ESEM chamber.[21] Because of the higher hydrophilicity of the nanotubes, compared to the sample holder, and their curvature, water condenses preferentially inside them rather than on the substrate (stainless steel) or on the outer surface of the nanotubes.[21] The ability to observe and control water condensation inside nanochannels using ESEM validated the potential application of carbon nanotubes as tools for drug delivery and other nanofluidic applications.[8,9,24]

* Corresponding author. E-mail: kkornev@clemson.edu.
† Drexel University.
‡ Clemson University.
§ Current address: New Jersey Center for Biomaterials, Rutgers University, 145 Bevier Road, Piscataway, New Jersey 08854.

(1) Whitby, M.; Quirke, N. *Nat. Nanotechnol.* **2007**, *2*, 87.
(2) Meldrum, D. R.; Holl, M. R. *Science* **2002**, *297*, 1197.
(3) Kouklin, N. A.; Kim, W. E.; Lazareck, A. D.; Xu, J. M. *Appl. Phys. Lett.* **2005**, *87*, 173901.
(4) Cai, D.; Mataraza, J. M.; Qin, Z. H.; Huang, Z.; Huang, J.; Chiles, T. C.; Carnahan, D.; Kempa, K.; Re, Z. *Nat. Methods* **2005**, *2*, 449.
(5) Supple, S.; Quirke, N. *Phys. Rev. Lett.* **2003**, *90*, 214501.
(6) Baughman, R. H.; Zhakidov, A. A.; deHeer, W. A. *Science* **2002**, *297*, 787.
(7) Dresselhaus, M. S., Dresselhaus, G. & Eklund, P. C. *Science of Fullerenes and Carbon Nanotubes*;Academic Press: San Diego, 1996.
(8) Korneva, G.; Ye, H.; Gogotsi, Y.; Halverson, D.; Friedman, G.; Bradley, J.-C.; Kornev, K. G. *Nano Lett.* **2005**, *5*, 879.
(9) Freedman, J. R.; Mattia, D.; Korneva, G.; Gogotsi, Y.; Friedman, G.; Fontecchio, A. K. *Appl. Phys. Lett.* **2007**, *90*, 103108.
(10) Gelb, L. D.; Gubbins, K. E.; Radhakrishnan, R.; Sliwinska-Bartkowiak, M. *Rep. Prog. Phys.* **1999**, *62*, 1573.
(11) Kornev, K. G.; Shingareva, I. K.; Neimark, A. N. *Adv. Colloid Interface Sci.* **2002**, *96*, 143.
(12) Neimark, A. V.; Ruetsch, S.; Kornev, K. G.; Ravikovitch, P. I. *Nano Lett.* **2003**, *3*, 419.
(13) Holt, J. K.; Park, H. G.; Wang, Y.; Stadermann, M.; Artyukhin, A. B.; Grigoropoulos, C. P.; Noy, A.; Bakajin, O. *Science* **2006**, *312*, 1034.
(14) Majumder, M.; Chopra, N.; Andrews, R.; Hinds, B. J. *Nature* **2005**, *438*, 44.
(15) Kolesnikov, A. I.; Zanotti, J. M.; Loong, C. K.; Thiyagarajan, P.; Moravsky, A. P.; Loutfy, R. O.; Burnham, C. J. *Phys. Rev. Lett.* **2004**, *93*, 035503.
(16) Maniwa, Y.; Kataura, H.; Abe, M.; Udaka, A.; Suzuki, S.; Achiba, Y.; Kira, H.; Matsuda, K.; Kadowaki, H.; Okabe, Y. *Chem. Phys. Lett.* **2005**, *401*, 534.
(17) Byl, O.; Liu, J. C.; Wang, Y.; Yim, W. L.; Johnson, J. K. & J. T.; Yates, J. *J. Am. Chem. Soc.* **2006**, *128*, 12090.
(18) Naguib, N.; Ye, H.; Gogotsi, Y.; Yazicioglu, A. G.; Megaridis, C. M.; Yoshimura, M. *Nano Lett.* **2004**, *4*, 2237.
(19) Ye, H.; Naguib, N.; Gogotsi, Y.; Yazicioglu, A.; Megaridis, C. M. *Nanotechnology* **2004**, *15*, 232.
(20) Kim, B. M.; Sinha, S.; Bau, H. H. *Nano Lett.* **2004**, *4*, 2203.

10.1021/la802684q CCC: $40.75
Published on Web 01/26/2009

However, one of the most interesting aspects of this work, which has been unexplained thus far, was the observed mechanical deformation of the CNT walls during the formation of a water film inside the CNT cavity. The deformation of bulk-compliant materials such as aerogels has been reported in the literature.[25−27] Some interesting deformation scenarios for aerogels have been suggested and studied experimentally in refs 25 and 26. Tubular structures such as nanotubes stay outside of these aerogel-like materials, and the adsorption-induced deformations are still poorly understood, though general phenomenological approaches to describe these deformations have been published.[25−29] In this study, we simultaneously monitor the nanotube deformation and film morphology, which allows us to reveal the key mechanisms of adsorption-induced deformations.

This nanotube deformation should be distinguished from the deformation caused by nanotube coiling when the nanotube buckles, loops, or folds on itself axially.[30,31] Elegant wetting experiments and comprehensive theory reported in refs 30 and 32 provide important evidence of the significance of the capillary forces that can induce the buckling of flexible fibrous structures. All fiberlike materials experience this buckling because of their flexibility: the thinner the fiber, the easier it buckles. In the buckling phenomenon discussed in refs 30 and 32, the change in the nanotube or fiber length is negligible. In contrast, an apparent change in nanotube diameter is visible in our experiments, wheras the change in the nanotube length is not. Therefore, this radial deformation is a manifestation of the anisotropic properties of the nanotube.

As is the case with many of the characterization aspects of carbon nanotubes, determining their mechanical properties is a challenge because of their dimensions. The first experimental report of the Young's modulus of individual multiwalled carbon nanotubes was performed using high-resolution TEM, where thermal vibrations of the CNT were measured and an elastic modulus of 1.8 TPa was estimated.[33] Similar experiments were performed on single-walled carbon nanotubes, which yielded a Young's modulus value of 1.25 TPa.[34] However, Salvetat et al. also showed that whereas the modulus for structurally ordered multiwalled CNT, synthesized by the arc-discharge method, was ∼810 GPa, disordered CNT, synthesized by catalytic thermal decomposition, had much lower elastic moduli of 10−50 GPa.[35] These results demonstrated the extremely high mechanical integrity of some types of carbon nanotubes and illustrated the fact that these properties depend not just on size but also on wall structure, which can be varied by changing the synthesis process parameters.

Aside from extremely high tensile moduli, buckling and radial deformation of carbon nanotubes have also been reported. For example, high-resolution TEM has been used to demonstrate the bending and flexibility of single-walled and multiwalled carbon nanotubes under mechanical load.[36,37] Furthermore, Ruoff et al. observed the radial deformation of CNTs by van der Waals forces;[38] specifically, by TEM measurements, it was shown that van der Waals forces between adjacent multiwalled carbon nanotubes were so strong that their cylindrical shape was distorted, and flattening of the CNTs occurred. A similar change in the cross-sectional shape caused by the interaction between the tubes was also observed for much larger tubes made by chemical vapor deposition (CVD), analogous to the ones studied in this work.[21] Similarly, using atomic force microscopy and molecular simulations, it has been shown that the nanotubes can be deformed by van der Waals interactions with a flat substrate.[39] To the best of our knowledge, the mechanics of adsorption-induced deformations of nanotubular materials has not yet been discussed in the literature.

In this article, we present a quantitative analysis of the radial and circumferential deformations of carbon nanotubes induced by the condensation of water vapor.

Results and Discussion

During the experiments, water vapor from the ESEM chamber entered and filled the CNT, primarily by diffusion of the water molecules. As the vapor pressure inside the CNT increased, commensurate with an increase in the vapor pressure inside the chamber, we observed vapor condensation inside the CNTs below the equilibrium saturation pressure. During the onset of condensation, the formation of a thin layer of water on the inner walls of the CNT occurred. This experiment was performed at 4 °C, for which the saturation vapor pressure is 6.2 Torr; condensation occurred inside the CNT at 5.6 Torr. More exciting, however, is the observed deformation or apparent decrease in diameter of the CNT upon condensation.

One might argue that the observed deformation of CNT upon the formation of a liquid film[21] could have been influenced by intermolecular interactions between the CNT and the stainless steel substrate. Therefore, an experiment was performed in which the membrane was cracked so that the CNTs on the outer surface were partially released (i.e., each CNT was partially suspended as a cantilever, held at one end by the supporting membrane, as shown in the schematics in Figure 1a,b and in the ESEM image in Figure 1c). As observed with the CNTs on the stainless steel substrate, the onset of condensation within the CNTs attached to the membrane occurred by the formation of a thin film of water inside the CNT and resulted in a decrease in diameter of the CNTs, as shown in Figure 1d,e. Therefore, we were able to corroborate that the deformation of these CNT is, in fact, independent of the substrate and characteristic of the nanotube itself. An analysis of the wall structure of the CNTs, by transmission electron microscopy, revealed that the CNTs have a disordered wall structure and that there is a lack of the organized graphitic wall structure of traditional MWNTs (Figure 1f).

The deformation of the CNT, interpreted by a decrease in diameter, is shown in Figure 2, where the decrease in diameter of the CNT is plotted as a function of pressure as condensation and film formation occur. It is important to note how the decrease in CNT diameter occurs immediately upon formation of the thin

(21) Rossi, M. P.; Ye, H.; Gogotsi, Y.; Babu, S.; Ndungu, P.; Bradley, J.-C. *Nano Lett.* **2004**, *4*, 989.
(22) Donald, A. M. *Nat. Mater.* **2003**, *2*, 511.
(23) Rossi, M. P.; Gogotsi, Y. *Microsc. Anal.* **2004**, *18*, 9.
(24) Schrlau, M. G.; Falls, E. M.; Ziober, B. L.; Bau, H. H. *Nanotechnology* **2008**, 19.
(25) Scherer, G. W.; Smith, D. M.; Stein, D. *J. Non-Cryst. Solids* **1995**, *186*, 309.
(26) Reichenauer, G.; Scherer, G. W. *Colloids Surf., A* **2001**, *187*, 41.
(27) Herman, T.; Day, J.; Beamish, J. *Phys. Rev. B* **2006**, 73.
(28) Chernyak, Y. B.; Leonov, A. I. *J. Colloid Interface Sci.* **1986**, *113*, 504.
(29) White, L. R. *J. Colloid Interface Sci.* **2003**, *258*, 82.
(30) Cohen, A. E.; Mahadevan, L. *Proc. Natl. Acad. Sci. U.S.A.* **2003**, *100*, 12141.
(31) Lourie, O.; Cox, D. M.; Wagner, H. D. *Phys. Rev. Lett.* **1998**, *81*, 1638.
(32) Bico, J.; Roman, B.; Moulin, L.; Boudaoud, A. *Nature* **2004**, *432*, 690.
(33) Treacy, M. M. J.; Ebbesen, T. W.; Gibson, J. M. *Nature* **1996**, *381*, 678.
(34) Krishnan, A.; Dujardin, E.; Ebbesen, T. W.; Yanilios, P. N.; Treacy, M. M. J. *Phys. Rev. B* **1998**, *58*, 14013.
(35) Salvetat, J.-P.; Kulik, A. J.; Bonard, J. M.; Briggs, G. A. D.; Stöckli, T.; Méténier, K.; Bonnamy, S.; Béguin, F.; Burnham, N. A.; Forró, L. *Adv. Mater.* **1999**, *11*, 161.
(36) Iijima, S.; Brabec, C.; Maiti, A.; Bernholc, J. *J. Chem. Phys.* **1996**, *104*, 2089.
(37) Despres, J. F.; Daguerre, E.; Lafdi, K. *Carbon* **1995**, *33*, 87.
(38) Ruoff, R. S.; Tersoff, J.; Lorents, D. C.; Subramoney, S.; Chan, B. *Nature* **1993**, *364*, 514.
(39) Hertel, T.; Walkup, R. E.; Avouris, P. *Phys. Rev. B* **1998**, *58*, 13870.

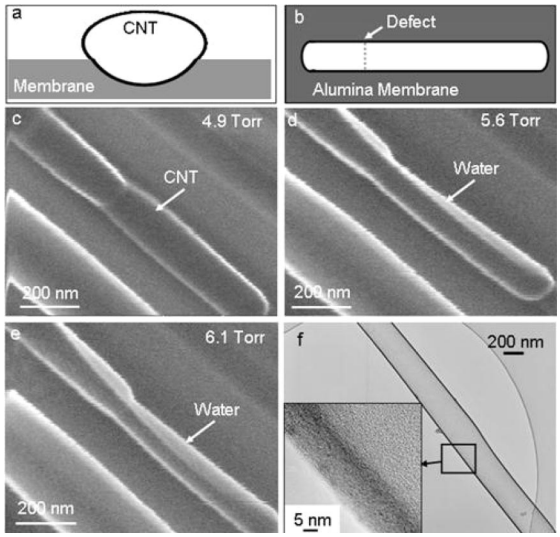

Figure 1. Deformation of carbon nanotubes in an alumina membrane. (a) Schematic showing the cross section of an individual CNT still partially attached to the membrane. (b) Schematic showing a top view of a CNT still partially attached to the membrane, where the dotted line shows an imperfection of the nanotube that was already present before experimentation. (c) ESEM image of CNT attached to the membrane before condensation. (d) ESEM image showing how, upon condensation, a thin film of water forms inside the CNT and deformation of the CNT begins. (e) ESEM image showing how film thickness increases as a result of an increase in the condensation of water within the CNT with an increase in pressure in the ESEM chamber. The experiment was carried out at 4 °C. Notice how condensation occurred before the saturation pressure (6.2 Torr) at that temperature. (f) TEM image showing the length and disordered wall structure (inset) of an individual CNT.

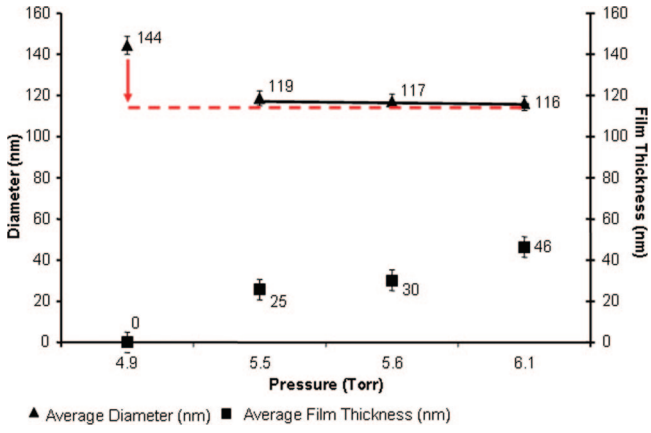

Figure 2. Decrease in CNT diameter with an increase in film thickness as the pressure increases in the ESEM chamber as condensation occurs. The dotted line shows the sudden decrease in CNT diameter immediately upon formation of the water film; the solid line shows how the CNT diameter remains constant even upon an increase in film thickness.

film of water (---) and the CNT diameter remains constant (−) while the film thickness increases as condensation continues.

Mechanism of Nanotube Shrinkage. Because the condensation of water inside CNTs initiates with the development of a liquid film and is followed by the formation of a meniscus, it can be described using the Kelvin relation for capillary condensation[40−42]

$$P_c = \left(\frac{\kappa T}{\upsilon}\right) \ln\left(\frac{P_o}{P_v}\right) \quad (1)$$

where P_c represents the difference between pressure in the vapor, P_v, and pressure in the water film, P_w, ($P_c = P_v - P_w$), κ is Boltzmann's constant, T is temperature, υ is the water molecular volume, and P_o is the saturation pressure for a planar vapor/liquid interface.

The pressure difference induced by the formation of a thin water film of thickness h inside a CNT of radius R can be estimated using the generalized Young−Laplace equation[11]

$$P_c = P_v - P_w = \left[\frac{\gamma}{(R-h)} + \Pi\right] \quad (2)$$

where γ is the surface tension and $\Pi = \Pi(h)$ is the term for an additional pressure known to exist in nanometer-thick films due to uncompensated surface forces acting at the liquid/vapor and liquid/solid interfaces.[43−45] For wetting fluids, this extra pressure is typically positive and is called the disjoining pressure to reflect the tendency of a precursor nanofilm to spread ahead of the droplet to enlarge its thickness spontaneously.[44,45]

As can be seen from eq 2, because of the simultaneous action of the disjoining and capillary pressures, the pressure in the liquid is lower than the pressure in the vapor. This spontaneous decrease in pressure between the vapor and the liquid acts to deform the nanotube walls. Thus, both the surface tension and the disjoining pressure tend to decrease the nanotube radius.

The simultaneous action of the surface tension and disjoining pressure is illustrated by the following model. Assume that the tube is an elastic shell. We introduce the radius of the water/vapor interface as $r = R - e$ and the radius of the deformed nanotube as $R_{def} = R - H$, where e is an apparent thickness of the liquid film measured from the nondeformed wall and H is the displacement of the nanotube wall. Therefore, the thickness of the liquid film covering the deformed nanotube is $h = e - H$. Appreciable deformations of the nanotubes were observed when the thickness of the liquid film was much smaller than the nanotube radius. We thus employ the thin film approximation $(h)/(R) \ll 1$, $(H)/(R) \ll 1$. Within this approximation, the conditions for mechanical equilibrium of the vapor/water interface and the nanotube are written as

$$-\gamma + (P_v - P_w)R - R\Pi(h) = 0 \quad (3)$$

and

$$\Sigma - (P_v - P_w)R + R\Pi(h) = 0 \quad (4)$$

where Σ is the circumferential tension in the nanotube associated with the hoop stress.[46] Equation 3 is the limiting case of eq 2 as h tends to zero. Both eqs 3 and 4 can be interpreted as the conditions of mechanical equilibrium of a cylindrical vessel with the circumferential tensions γ and Σ compressed by the pressure $(P_v - P_w) - \Pi(h)$.[46]

Summing up eqs 3 and 4, we find that the effect of capillary and disjoining pressures can be reduced to an additional force compressing the nanotube in the circumferential direction:

$$\Sigma = \gamma \quad (5)$$

In turn, the tension $\Sigma = \sigma_{\theta\theta} t$ is expressed through the circumferential elastic stress, $\sigma_{\theta\theta}$, and the nanotube thickness,

(40) Thomson, W. T. *Philos. Mag.* **1871**, *42*, 448–452.
(41) Fisher, L. R.; Israelachvili, J. N. *Nature* **1979**, *277*, 548.
(42) Mitropoulos, A. C. *J. Colloid Interface Sci.* **2008**, *317*, 643.
(43) Derjaguin, B. V. *Acta Physicochim. URSS* **1940**, *12*, 181.
(44) Derjaguin, B. V., Churaev, N. V. & Muller, V. M. *Surface Forces*; Plenum Press, Consultants Bureau: New York, 1987.
(45) Israelachvili, J. *Intermolecular and Surface Forces: With Applications to Colloidal and Biological Systems*, 2nd ed; Academic Press: London, 1994.
(46) Flugge, W. *Stresses in Shells*; Springer: Berlin, 1973.

t. In the theory of thin anisotropic shells,[46,47] the radial stress in the shell is proven to be negligibly small, and as shown in Appendix A, the axial stress is also negligibly small compared to the circumferential stress, $\sigma_{\theta\theta}$. Therefore, Hooke's law for the nanotube material takes the form $\varepsilon_{\theta\theta} = \sigma_{\theta\theta}/E_{\theta\theta}$, where $E_{\theta\theta}$ is the circumferential Young's modulus. (See Appendix A for details.) The circumferential strain, $\varepsilon_{\theta\theta}$, is written as $\varepsilon_{\theta\theta} = (R_{\text{def}} - R)/R$, where R_{def} is the nanotube radius after deformation. Using eq 5 and approximate Hooke's law $\varepsilon_{\theta\theta} = \sigma_{\theta\theta}/E_{\theta\theta}$, the radius R_{def} is obtained as

$$R_{\text{def}} = R - \frac{R\gamma}{tE_{\theta\theta}} \tag{6}$$

The important conclusion is that the radial deformation of the nanotube should be constant whenever our approximation, $h \ll R$, $t \ll R$, holds. Our experimental results, summarized in Figure 2, show that the deformation of the nanotube is almost constant during a broad range of vapor pressure variations. To estimate the Young's modulus, we use the data from Figure 2 and take $t = 20$ nm, $R = 72$ nm, $R_{\text{def}} = 58.5$ nm, and $\gamma \cong 70$ mN/m. With these parameters, we obtain the circumferential Young's modulus $E_{\theta\theta} \cong 18.6$ MPa. If we take the Hencky strain $\varepsilon_{\theta\theta} = \ln(R_{\text{def}}/R)$, which is better suited to describe large deformation with almost no change in nanotube volume,[48] then the elastic module changes to $E_{\theta\theta}$=16.8 MPa. In both models, the circumferential Young's modulus is significantly lower than the axial modulus of CNTs produced by arc discharge and catalytic CVD methods.[35] This value would be higher for perfect nanotubes built of concentric carbon shells. The CVD tubes studied in this work, however, consist of graphite patches with the edge planes terminated by hydrogen.[49,50] However, it is important to stress that $E_{\theta\theta}$ is not just a parameter of the carbon material of the tube wall, but this is a characteristic of the shell structure. This explains why CVD carbon tips, similar to the ones described in this work, can be easily bent, kinked, buckled, and unbuckled with no damage, as was shown in ref 24.

Within the same approximation, $(h)/(R) \ll 1$, when nanotube deformation is constant, the variation in the film thickness follows eq 3 and is caused by the disjoining pressure term. Using eq 1, we can rewrite eq 3 in the form

$$\left(\frac{\kappa T}{\upsilon}\right)\ln\left(\frac{P_{\text{o}}}{P_{\text{v}}}\right) - \frac{\gamma}{R} = \Pi(h) \tag{7}$$

The experimental dependence $\Pi(h)$ is shown in Figure 3. Because a detailed analysis of film thickness variation versus vapor pressure was not possible with our instrument, it is difficult to assess the origin of surface forces responsible for film growth. Still, these results show that one can potentially use CVD nanotubes as a test bed for studying the properties of liquid films. Because nanotube deformation is mostly controlled by the surface tension of the condensed film, one can measure the surface tension of the adsorbed film using a nanotube with well-defined elastic properties. However, the adsorption properties of the nanofilm can be studied by monitoring the film thickness as a function of vapor pressure.

One more unusual phenomenon has been observed in our experiments, which deserves special attention.

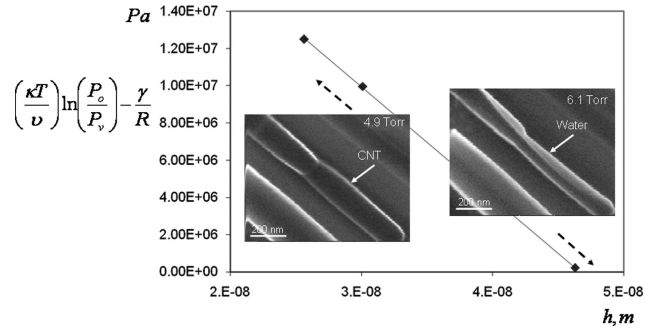

Figure 3. Graph of disjoining pressure as a function of h measured in meters. The line is approximated by the equation $\Pi = -6 \times 10^{14}\, h + 3 \times 10^7$ Pa.

Nanotube Buckling. Whereas the decrease in nanotube diameter occurs during the formation of thin films on the inner walls of the CNT, we also observed an apparent enlargement of the CNT diameter (1%−10%) once the vapor pressure had approached or surpassed the saturation pressure. At this pressure level, a full meniscus could be observed inside the CNT, as shown in Figure 4. We interpret this apparent enlargement of the CNT diameter upon filling with water as nanotube buckling. It is quite similar to the behavior predicted by Lévy[51] and Carrier[52] and is analyzed in detail in 53 and 54, where elastic rings, tubes, and shells undergo elastic buckling under an applied pressure.

For quantitative analysis of this buckling instability, we assume that the CNT has a circular cross section before deformation. We also assume that the axial stresses in the nanotube are incomparably smaller than the circumferential stresses, so the short nanotubes do not experience significant deformations in the axial direction and may be modeled as the Lévy−Carrier rings. Accordingly, the circumferential Young's modulus, $E_{\theta\theta}$, and the second moment of inertia for a rectangular plate, $I = t^3L/12$, where L is the nanotube length, should replace the corresponding Lévy−Carrier parameters.[46,51] Therefore, the flexural rigidity per unit length of the nanotube is written as $EI/L = E_{\theta\theta}t^3/12$. Applying the Lévy−Carrier criterion of the maximum applied pressure that the nanotubes can withstand, we write the critical pressure, P_{cr}, as defined in refs 51−54:

$$P_{\text{cr}} = \frac{(n^2 - 1)E_{\theta\theta}t^3}{12R^3} \tag{8}$$

When the short CNT, or ring in the theoretical case, becomes unstable at $P > P_{\text{cr}}$, the circular shape changes and is replaced by a wavelike shape with wavenumber n. In the case of the CNT, this wavenumber is likely to be 2, which corresponds to an ellipse.

Because our CNT diameters are large (100−200 nm), the surface molecular forces do not change the shape of the menisci appreciably. Neglecting the disjoining pressure effect for large menisci, the Kelvin equation can be written in the general case of nonspherical menisci as

$$\left(\frac{\kappa T}{\upsilon}\right)\ln\left(\frac{P_{\text{o}}}{P_{\text{v}}}\right) = 2\text{K}\gamma \tag{9}$$

where 2K is the sum of the two principal curvatures of the meniscus. Even when the tube sustains a significant deformation and the meniscus can no longer be considered to be semispherical,

(47) Lekhnitskii, S. G. *Theory of Elasticity of an Anisotropic Elastic Body*; Holden-Day: San Francisco, 1963.
(48) Hencky, H. *J. Rheol.* **1931**, *2*, 169.
(49) Mattia, D.; Rossi, M. P.; Kim, B. M.; Korneva, G.; Bau, H. H.; Gogotsi, Y. *J. Phys. Chem. B* **2006**, *110*, 9850.
(50) Mattia, D.; Bau, H. H.; Gogotsi, Y. *Langmuir* **2006**, *22*, 1789.
(51) Lévy, M. *J. Math.* **1884**, *3*, 7.
(52) Carrier, G. F. *J. Math. Phys.* **1947**, *26*, 94.
(53) Flaherty, J. E.; Keller, J. B.; Rubinow, S. I. *SIAM J. Appl. Math.* **1972**, *23*, 446.
(54) Tadjbakhsh, I.; Odeh, F. *J. Math. Anal. Appl.* **1967**, *18*, 59.

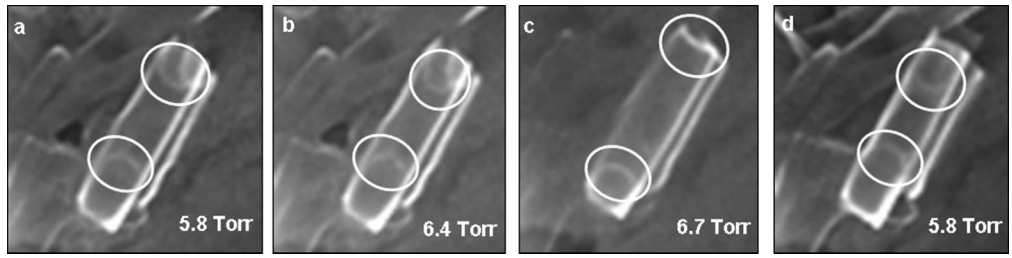

Figure 4. ESEM images of nanotubes exposed to vapor at different pressures. We show one cycle when the pressure was increased from 5.8 to 6.7 Torr and then decreased to 5.8 Torr. It is seen that the nanotube regained its diameter when the vapor pressure increased to 6.7 Torr. Note the meniscus sitting at the edge of the nanotube.

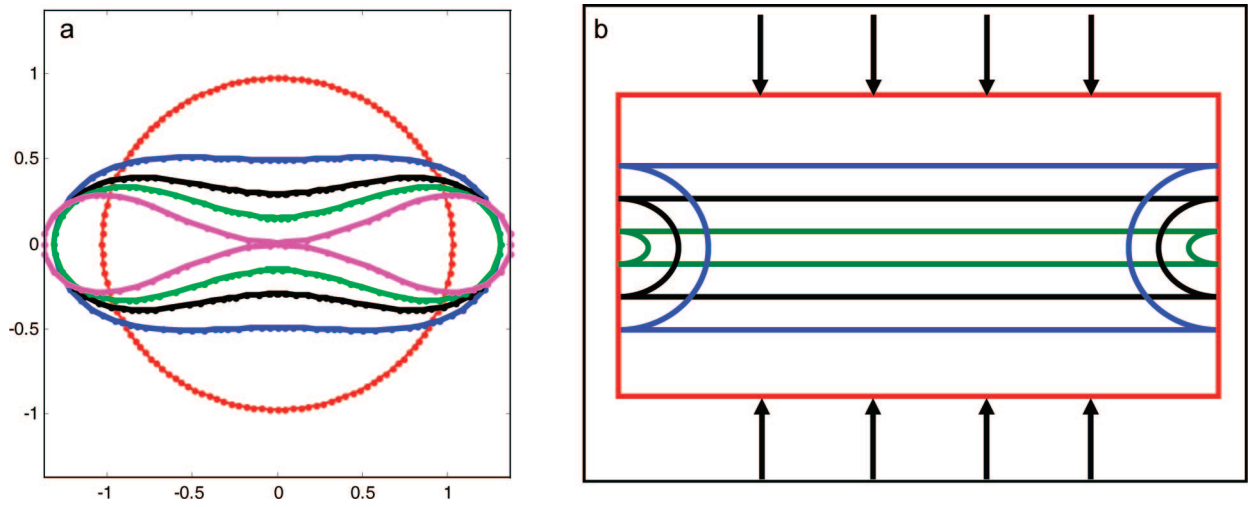

Figure 5. Carbon nanotube deformation with vapor pressure. (a) Cross-sectional view showing the deformation of a CNT by different vapor pressures; the CNT shape goes from circular (red) to elliptical and the CNT begins to compress when the menisci curvature increases. This phenomenon, under the ESEM, appears as a widening of the diameter of the CNT. (b) Side view of nanotubes in part a with menisci pictured as semicircles, where the red CNT has no meniscus. Arrows indicate the direction of deformation.

the generalized Kelvin equation (eq 9) is still applicable. Therefore, the left-hand side of eq 9, which is controlled by the pressure in the chamber, immediately imposes the capillary pressure. By combining eq 9 with eq 8, we state that for CNT deformation to occur the following condition must be met:

$$P_v < P_o \exp\left[\frac{-\upsilon E_{\theta\theta} t^3}{4\kappa T R^3}\right] \qquad (10)$$

When the vapor pressure becomes too high (during filling of the CNT, when menisci propagate toward the nanotube ends, or during emptying of the nanotubes, when flat menisci at the tube ends gradually transform into the curved menisci) and P_v becomes greater than the right-hand side of eq 10, the CNT deforms and becomes elliptical, as shown in Figure 5. This, under the ESEM, looks like an increase in the diameter of the CNT as we are observing it from the top.

Figure 5 illustrates a scenario of nanotube buckling. After normalizing the critical pressure by γ/R, we define the dimensionless critical pressure as $P = (3E_{\theta\theta}t^3)/([12\gamma R^2])$. Using the approach suggested in refs 53 and 54, we calculated the shapes of the nanotube at different P values. The red, undeformed CNT was obtained at $P = 3$. As the pressure increases (3.5 for the blue CNT, 4 for the black CNT, 4.5 for the green nanotube, and 5.27 for the pink CNT), the deformation of the CNT becomes more pronounced, and the shape of the CNT is more curved until, at $P = 5.27$, the top and bottom walls of the CNT actually meet.

In our experiments, we did not observe nanotube buckling to the point where the opposite sides of the wall touch each other. However, this scenario seems to be plausible, and we know from independent compression experiments with AFM that the nanotube wall is strong enough to support this load without fracturing. It is interesting to check our estimate of the Young's modulus using the buckling experiments. The criticality condition, eq 9, can be rewritten in the form $E_{\theta\theta} = -(4kTR^3/\upsilon t^3)\ln(P_v/P_0)$. Taking $\upsilon = 27 \times 10^{-30}$ m^3 for the molecular volume, $T = 277$ K for the temperature (controlled by the Peltier cooling stage in the ESEM chamber with a volume of 15 L), $P_v/P_0 = 0.9995$ for the relative pressure, and a ratio of the thickness of the CNT wall to the CNT radius defined as $(t)/(R) = (20)/(72)$, we estimate that the modulus of the CNT to be only about 13 MPa. Our estimate for the CVD CNT is in accord with that found from the analysis of nanotube deformations caused by the adsorbed film.

Carbon and other nanotubes were recently suggested to be used as nanoscale thermometers.[55] Recent studies measuring the radial elastic modulus of MWNT of smaller diameters (under 50 nm) also made by chemical vapor deposition[56] indicate a much higher value of ~20 GPa. The CVD CNT moduli are also lower than the 0.3−4 GPa values reported by Yu et al., who measured the radial deformability of individual MWNT with AFM,[57] or values obtained by Palaci et al., who also measured using AFM, which ranged from 20−40 GPa.[58] In fact, our measurements are similar to those previously reported for porous carbon materials

(55) Li, Y. B.; Bando, Y.; Goldberg, D.; Liu, Z. W. *Appl. Phys. Lett.* **2003**, *83*, 999.
(56) Muthaswami, L.; Zheng, Y.; Vajtai, R.; Shehkawat, G.; Ajayan, P.; Geer, R. E. *Nano Lett.* **2007**, *7*, 3891.
(57) Yu, M.-F.; Kowalewski, T.; Ruoff, R. S. *Phys. Rev. Lett.* **2000**, *85*, 1456.

and carbon foams.[59] Our results demonstrate not only a novel technique for measuring CNT deformability and elasticity, but we also report on much more elastic nanotubes that have the potential to be much more sensitive to vapor pressure changes in the presence of gases and humidity in the environment.

The extreme sensitivity of the nanotubes to vapor pressure shown in our work renders them potential humidity or pressure sensors for the detection of minute pressure changes. For example, by forming a micrometer-thick bundle or fiber from these nanotubes, one can easily detect bundle deformations upon vapor condensation.[12,60] We expect that the presented observations and suggested theory will open up new areas of nanotube application. Because hollow nanofibers and nanotubes can be produced from different materials using the same template method, shells with different elastic properties can be designed and manufactured.

Conclusions

The condensation of water inside carbon nanotubes was accompanied by the formation of a thin film of water on the inner walls of the nanotubes at a pressure that is usually lower than the saturation vapor pressure for the corresponding flat water−vapor interface. Upon formation of this film, elastic deformation of the carbon nanotubes was observed by an apparent decrease in nanotube diameter. As pressure increased and a water plug formed inside the nanotubes, we also observed an apparent increase in nanotube diameter. We interpreted our experimental results by considering the nanotube to be an elastic shell. Radial shell deformations are shown to be mostly controlled by the surface tension of the condensed film, whereas the film thickness is controlled by the disjoining pressure due to surface forces. An apparent increase in the nanotube diameter is interpreted as the manifestation of the buckling phenomenon inherent in thin elastic shells. We analyze our experiments by modifying the Lévy classical analysis of pipe buckling by augmenting it with the Kelvin theory of capillary condensation. It appears that the buckling criterion does not depend on the shape of the meniscus in the nanotube. Therefore, the vapor pressure can be used as a bifurcation parameter specifying the tube shape after buckling. We derived the buckling condition that relates the relative pressure to the elastic and geometric parameters of the nanotube. The presented experimental and theoretical analyses of nanotube radial deformation and buckling show that the circumferential Young's moduli vary in the range of $E_{\theta\theta} \approx 13-18$ MPa.

Materials and Methods

CNTs for this study were produced by the noncatalytic chemical vapor deposition (CVD) of a hydrocarbon gas in a porous alumina membrane (Whatman Anodisc) with a nominal pore size of 200 nm ± 10%, using methods described previously.[21] The walls of the resulting CNTs are composed of small, disjointed graphene sheets, rich in functional groups, demonstrating transparency and high sensitivity to annealing temperature.[49,50] The wall thickness is 15−20 nm; after treatment in NaOH, which dissolves the alumina membrane, the CNTs are hydrophilic, with a contact angle of ∼44°.[49]

Contact angles were measured with high accuracy on CVD carbon films on planar substrates prepared under the same conditions as for the CNTs,[49,50] but estimates of the contact angle made using droplets of water condensing on CNTs inside ESEM had comparable values. The hydrophilicity plays an important role in water condensation. In the case of as-produced CVD nanotubes on a steel substrate, water condensation occurred preferentially inside the tubes because their contact angle was lower than that of the substrate. An increase in the hydrophobicity of CVD nanotubes by vacuum annealing led to water condensation on the substrate or between the tube and the substrate. Nanotubes were filled only after water flooded the substrate surface.[49]

Because of the highly irregular packing of graphene sheets of a few nanometers in size in the nanotube walls, the CVD-formed nanotubes have many defects[49] and thus are expected to have a lower stiffness and strength compared to those produced by arc discharge and catalytic CVD methods.[35]

Condensation and evaporation were induced and observed in carbon nanotubes using an FEI-XL30 environmental scanning electron microscope (ESEM). To induce condensation, the temperature was kept constant (1−4 °C) with the use of the Peltier cooling stage. The pressure in the ESEM chamber was increased slowly (∼0.1 °C/30−120 s) until condensation occurred near the saturation vapor pressure specific for the temperature used. Subsequently, the pressure was decreased slowly to induce evaporation.

Acknowledgment. We thank Dr. Haihui Ye for help with TEM image acquisition. We are thankful to Professor B. Layton for his comments after a thorough reading of the manuscript. M.P.R. was supported by an NSF graduate research fellowship. Additional support was provided by the NSF NIRT (grant CBET-0609062) and the Keck Foundation, and K.G.K. is supported by the NSF (grant CMMI 0826067) and the Department of Commerce through the National Textile Center (grant M08-CL10).

Appendix A

As a model of a liquid film of thickness h sitting on the inside surface of the nanotube of radius R, we consider the model where the film is pinned at the nanotube edge. In this case, the Derjaguin model of the liquid film[11] is written for the transition zone as

$$P_c = P_v - P_w = \frac{\gamma h''}{(1+h'^2)^{3/2}} + \frac{\gamma}{(R-h)(1+h'^2)^{1/2}} + \Pi(h) \tag{A1}$$

This equation can be integrated to give

$$-\frac{\gamma(R-h)}{\sqrt{1+u^2}} + \gamma R\cos\phi = -\int_0^h (R-h)(P_c - \Pi(h))\,dh \tag{A2}$$

where ϕ is the angle at which the film meets the nanotube edge. Far away from the nanotube edge, when the film approaches its equilibrium thickness h_0, eq A2 is transformed to

$$\gamma(R-h_0) - \gamma R\cos\phi = -\int_0^{h_0} (R-h)(P_c - \Pi(h))\,dh \tag{A3}$$

The second term in eq A3 is related to the force acting at the nanotube edge. Indeed, accounting for the restriction on the disjoining pressure, which guaranties the existence of wedge-type films $\Pi h/\gamma \to 0$ as $h \to 0$,[11] one can say that neither the disjoining pressure nor the water pressure contribute to the force balance at the edge. Hence, the force acting at the nanotube edge is given by the surface tension only:

$$\sigma_{zz} t = \gamma\cos\phi \tag{A4}$$

Thus, the compression stress acting on the nanotube edge is expressed through eq A3 as

(58) Palaci, I.; Fedrigo, S.; Brune, H.; Klinke, C.; Chen, M.; Riedo, E. *Phys. Rev. Lett.* **2005**, *94*, 175502.
(59) Min, G.; Zengmin, S.; Weidong, C.; Hui, L. *Carbon* **2007**, *45*, 141.
(60) Kornev, K. G.; Callegari, G.; Kuppler, J.; Ruetsch, S.; Neimark, A. V. *Phys. Rev. Lett.* **2006**, *97*, 188303.

$$\sigma_{zz} tR = \gamma(R - h_0) + \int_0^{h_0} (R - h)(P_c - \Pi(h))\, dh \quad \text{(A5)}$$

For very thin films, when $t \gg h_0$, we have $\sigma_{zz} \approx \gamma/t$. We can use this stress to estimate the associated deformations in the nanotube.

The nanotube is modeled as a thin anisotropic shell with a cylindrical symmetry that can be observed in many natural materials, and wood is the best example.[47] In this model, the radial (r) circumferential (θ), and axial (z) directions are the principal directions of nanotube anisotropy. When the nanotube is loaded by the pressure from the inside or a compression/extension load is acting in the z direction, all elements of the tube are deformed. Scaling arguments used in the theory of thin anisotropic shells suggest that we can neglect the radial stress as compared to the circumferential and axial stresses.[46] Therefore, for the loading considered in this paper, Hooke's law is written as[47]

$$\varepsilon_{\theta\theta} = \frac{\sigma_{\theta\theta}}{E_{\theta\theta}} - \frac{\upsilon_{z\theta}\sigma_{zz}}{E_{zz}}, \varepsilon_{zz} = \frac{\sigma_{zz}}{E_{zz}} - \frac{\upsilon_{\theta z}\sigma_{\theta\theta}}{E_{\theta\theta}},$$

$$\varepsilon_{rr} = -\frac{\upsilon_{\theta r}\sigma_{\theta\theta}}{E_{\theta\theta}} - \frac{\upsilon_{zr}\sigma_{zz}}{E_{zz}} \quad \text{(A6)}$$

where ε is the strain, σ is the stress, the subscript θ corresponds to the circumferential direction, z corresponds to the axial direction, and r corresponds to the radial direction. E represents the Young's moduli of the nanotube, and υ represents the Poisson ratios, which are defined as $\upsilon_{z\theta} = -\varepsilon_{zz}/\varepsilon_{\theta\theta}$, when the tube is stressed in the θ direction and other stresses are zero (i.e., when $\sigma_{\theta\theta} \neq 0$ and $\sigma_{rr} = \sigma_{zz} = \sigma_{ij} = 0$ (where indexes i and j correspond to $i, j = r, \theta, z$). $\upsilon_{\theta r} = -\varepsilon_{\theta\theta}/\varepsilon_{rr}$ when the tube is stressed in the r direction and other stresses are zero, and $\upsilon_{\theta z} = -\varepsilon_{\theta\theta}/\varepsilon_{zz}$ when the tube is stressed in the z direction and other stresses are zero.

From eqs 5 and A4, it becomes evident that the circumferential and axial stresses have the same order of magnitude: $\sigma_{\theta\theta}, \sigma_{zz} \approx \gamma/t$. Therefore, if we assume that the circumferential Young's modulus is significantly smaller than the axial modulus, then the stress-to-modulus ratios will follow the strong inequality $\sigma_{\theta\theta}/E_{\theta\theta} \gg \sigma_{zz}/E_{zz}$. Hence, Hooke's law can be approximated as $\varepsilon_{\theta\theta} = \sigma_{\theta\theta}/E_{\theta\theta}$, which leads to eq 6.

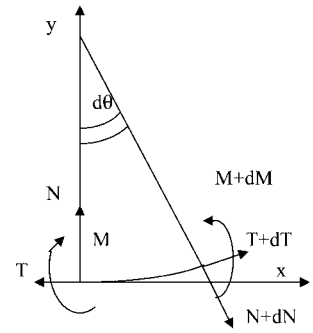

Figure B1. Force distribution diagram showing the variation of forces and moments within the elementary section dθ. All forces are counted per unit length along the tube.

Appendix B: Nanotube Buckling

If a nanotube is modeled as a thin elastic sheet, then its bending features can be described by applying the Euler−Bernoulli elastica equations[54] (see the explanations of terms in Figure B1)

$$\frac{dT}{ds} + Nk = 0, \frac{dN}{ds} + Tk - P_c = 0,$$

$$\frac{dM}{ds} - N = 0, M = \frac{E_{\theta\theta} t^3}{12}(k - k_0) \quad \text{(B1)}$$

where T is the tangential component of the force acting along the tube wall, N is the normal component of the force, M is the bending moment, $k = d\theta/ds$ is the curvature, k_0 is the initial curvature of the nanotube, where for a circular nanotube of radius R we have $k_0 = 1/R$, and s is the arc length. Linearization of these equations about the solution corresponds to the circular shape of the nanotube, which leads to eq 8. Numerical solutions shown in Figure 5 have been found by using the approach described in refs 53 and 54. Starting from the weakly nonlinear solution of ref 54 and using the method of parametric continuation, we solved eq B1 in Matlab.

LA802684Q